Available online at www.sciencedirect.com
SCIENCE DIRECT®
Journal of Power Sources 147 (2005) 107–115
JOURNAL OF POWER SOURCES
www.elsevier.com/locate/jpowsour

Crystallization kinetics of a solid oxide fuel cell seal glass by differential thermal analysis

Narottam P. Bansal*, Eleanor A. Gamble

National Aeronautics and Space Administration, Glenn Research Center, Cleveland, OH 44135, USA

Received 29 December 2004; accepted 14 January 2005
Available online 11 March 2005

Abstract

Crystallization kinetics of a barium–calcium aluminosilicate glass (BCAS), a sealant material for planar solid oxide fuel cells (SOFC), have been investigated by differential thermal analysis (DTA). From variation of DTA peak maximum temperature with heating rate, the activation energy for glass crystallization was calculated to be 259 kJ/mol using a kinetic model. Development of crystalline phases on thermal treatments of the glass at various temperatures has been followed by powder X-ray diffraction. Microstructure and chemical composition of the crystalline phases were investigated by scanning electron microscopy and energy dispersive spectroscopic (EDS) analysis. $BaSiO_3$ and hexacelsian ($BaAl_2Si_2O_8$) were the primary crystalline phases whereas monoclinic celsian ($BaAl_2Si_2O_8$) and (Ba_xCa_y)SiO_4 were also detected as minor phases. Needle-shaped $BaSiO_3$ crystals are formed first, followed by the formation of other phases at longer times of heat treatments. The glass does not fully crystallize even after long-term heat treatments at 750–900 °C. Devitrification of the glass seal over a long period of time during operation of the SOFC would generate thermal stresses in the seal and may have adverse effects on its mechanical performance. This may lead to cracking of the seal, resulting in mixing of the fuel and the oxidant gases.

Keywords: Solid oxide fuel cell; Seals; Glass; Devitrification; Activation energy; Differential thermal analysis

1. Introduction

Solid oxide fuel cells (SOFCs) [1] are being developed for a broad range of applications including portable electronic devices, automobiles, power generation, aeronautics, etc. The salient features of SOFC are all solid construction and high-temperature electrochemical reaction based operation, resulting in clean and efficient power generation from a variety of fuels. SOFCs of two different designs, tubular and planar, are currently under development. Planar SOFCs offer several advantages such as simple manufacturing and relatively short current path resulting in higher power density and efficiency. However, planar SOFCs require hermetic seals to separate and contain fuel and oxidant within the cell and to bond cell components together. The requirements for SOFC sealing materials are severe since the cells will operate at 600–1000 °C for thousands of hours, with sealing materials exposed to both oxidizing and reducing conditions. The seals must be chemically and mechanically compatible with different oxide and metallic cell components and should be electrically insulating. Also, they must survive cycling between room and operational temperatures. Various glass and glass-ceramics based on borates, phosphates and silicates are being examined [2–8] for SOFC seals. Silicate glasses are expected to perform superior to the borate and phosphate glasses. A barium–calcium aluminosilicate (BCAS) glass composition appears to be quite promising [2]. Chemical compatibility of this BCAS glass with metallic interconnects has been investigated [9,10].

The main objective of the present work was to investigate the crystallization kinetics of the BCAS glass. Another objective was to study the formation of crystalline phase(s)

* Corresponding author. Tel.: +1 216 433 3855; fax: +1 216 433 5544.
E-mail address: Narottam.P.Bansal@nasa.gov (N.P. Bansal).

0378-7753/$ – see front matter.
doi:10.1016/j.jpowsour.2005.01.010

in the glass under conditions, which are similar to those at which the solid oxide fuel cell is sealed and operated.

2. Experimental methods

A barium–calcium aluminosilicate glass of composition (mol%) $35BaO–15CaO–5Al_2O_3–10B_2O_3–35SiO_2$ was obtained in the form of powder and frit from a commercial vendor. The glass powder had an average particle size of 14.2 μm.

Crystallization kinetics of the BCAS glass powder were studied by differential thermal analysis (DTA) using a Netzsch STA 409C system interfaced with a computerized data acquisition and analysis system. Glass samples were contained in alumina cups. DTA scans were recorded from room temperature to 1000–1100 °C in flowing dry argon at various heating rates of 2–40 °C/min. Glass transition temperatures (T_g) and crystallization peak maximum temperatures (T_p) were obtained from the DTA scans.

The development of crystalline phases in the BCAS glass was investigated by isothermal heat treatments of bulk and powder samples in an electric furnace in air. The samples were heat treated for 1–100 h at various temperatures from 700 to 1000 °C. Phases crystallizing in the heat treated glass powder were identified from powder X-ray diffraction (XRD) patterns recorded at room temperature using a step scan procedure (0.03°/2θ step, count time 0.4 s) on a Philips ADP-3600 automated diffractometer equipped with a crystal monochromator employing Cu Kα radiation. Microstructures of the polished cross-sections of heat treated bulk glass specimens were observed using a JEOL JSM-840A scanning electron microscope (SEM). Prior to analysis, a thin layer of Pt or carbon was evaporated onto the SEM specimens for electrical conductivity. Qualitative X-ray elemental analysis of various phases was carried out using a Kevex Delta thin window energy dispersive spectrometer (EDS) and analyzer.

3. Theoretical background

The kinetics of phase transformation, such as crystallization of a glass, at a constant temperature can be described by the Johnson–Mehl–Avrami (JMA) equation [11,12]:

$$-\ln(1-x) = (kt)^n \tag{1}$$

where x is the volume fraction of the glass crystallized after time t, n the dimensionless Avrami exponent which is related to the morphology of crystal growth, and k is the reaction rate constant. The temperature dependence of k (at least within narrow temperature ranges) can be expressed by the Arrhenius equation:

$$k = \upsilon \exp\left[-\frac{E}{RT}\right] \tag{2}$$

where E is the effective overall activation energy for the transformation process, υ an effective frequency factor which is a measure of the probability that a molecule having energy E participates in the transformation, R the gas constant, and T is the absolute reaction temperature.

During a non-isothermal DSC or DTA scan, the sample temperature changes linearly with time at a rate θ (=dT/dt):

$$T = T_i + \theta t \tag{3}$$

where T_i is the initial temperature. In Eq. (1) the right-hand side corresponds to growth in volume of crystal nuclei. However, for the non-isothermal case the rate constant changes continuously with time due to the changing temperature, so that the JMA relation must be written as:

$$-\ln(1-x) = \left(\int_0^t k(t)\,\mathrm{d}t\right)^n \tag{4}$$

If at each temperature, the deflection of the DSC or DTA trace from its baseline is proportional to the instantaneous crystallization rate (Borchard assumption [13]), then the rate of sample transformation is maximum at the peak of the crystallization exotherm. Bansal et al. [14–16] have earlier shown that the temperature T_p of the crystallization peak changes with heating rate θ according to the relation:

$$\ln\left(\frac{T_p^2}{\theta}\right) = \ln\left(\frac{E}{R\upsilon}\right) + \frac{E}{RT_p} \tag{5}$$

Hence a plot of $\ln(T_p^2/\theta)$ versus $1/T_p$ should be linear with a slope of E/R and an intercept $[\ln(E/R) - \ln\upsilon]$. Eq. (5) is based on the assumption that at the temperature corresponding to the maximum in the crystallization exothermic peak, the degree of crystallization attains the same specific value independent of the heating rate. Earlier studies have shown that the crystallization kinetic parameters obtained by isothermal and non-isothermal DSC using Eq. (5) are in good agreement, particularly when both studies are carried out in the same temperature range.

Values of the Avrami parameter n can be evaluated from the non-isothermal data using an expression derived by Piloyan et al. [17] which is valid in the range $0 < x < 0.2$:

$$\frac{\mathrm{d}\ln(\Delta y)}{\mathrm{d}(1/T)} = -\frac{nE}{R} \tag{6}$$

where (Δy) is the vertical displacement at temperature T of the DSC or DTA crystallization exotherm from the baseline. The Avrami parameter n gives an indication of the crystal growth mechanism in the glass.

4. Experimental results

4.1. Physical properties of glass

Chemical composition of the BCAS glass and some of its physical, thermal and mechanical properties are

Table 1
Properties of BCAS glass

Property	Value
Composition	35BaO–15CaO–5Al_2O_3–10B_2O_3–35SiO_2 (mol%) 56.4BaO–8.8CaO–5.4Al_2O_3–7.3B_2O_3–22.1SiO_2 (wt.%)
Average particle size	14.2 μm
Density	3.88 g/cm^3
Glass transition temperature	619 °C
Dilatometric softening point	682 °C
Coefficient of thermal expansion	10.5×10^{-6} °C^{-1} (RT–500 °C); 11.8×10^{-6} °C^{-1} (20–800 °C)
Young's modulus	72 GPa
Microhardness	5.96 GPa
Flexure strength	50 MPa
Fracture toughness	0.56 MPa $m^{1/2}$

listed in Table 1. The T_g value of 619 °C for this glass is below the SOFC operating temperature. The coefficient of thermal expansion (CTE) of this glass ($10.5–11.8 \times 10^{-6}$ °C^{-1}) is in the same range as the CTE of other SOFC components: cathode, anode, electrolyte and interconnect.

4.2. Crystallization kinetics by DTA

DTA scans for BCAS glass were recorded at various heating rates from 2 to 40 °C/min. Typical scans at heating rates of 10 and 40 °C/min are shown in Fig. 1(a and b), respectively. The first endothermic peak at ~650–680 °C is due to the glass transition and the broad exothermic peak is due to crystallization of the glass. The second endothermic peak

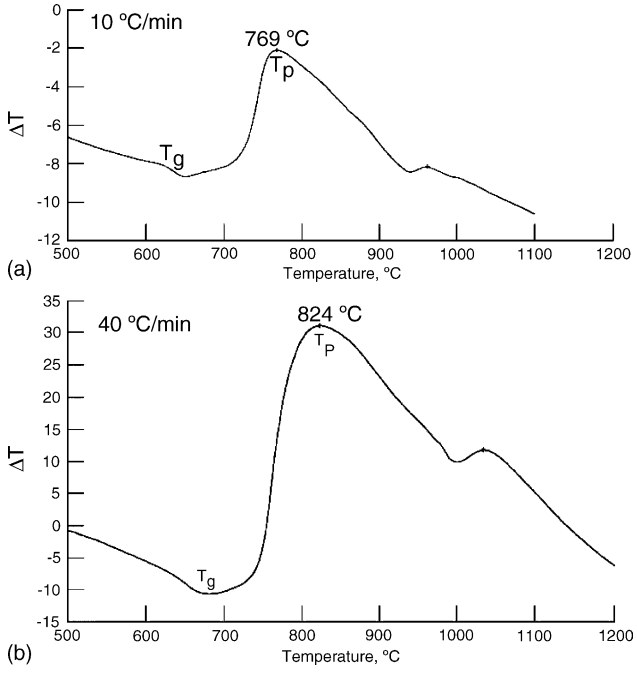

Fig. 1. DTA thermograms of BCAS glass powder at heating rate of (a) 10 °C/min and (b) 40 °C/min in air.

Table 2
Effect of heating rate on DTA crystallization peak temperatures (T_p) of BCAS glass

Scan rate (°C/min)	T_p (°C)
2	726.9
5	749.3
10	769.0
20	785.7
30	814.2
40	823.6

at ~940–1000 °C is from the melting of crystalline phases and/or residual glass. Influence of scan rate on crystallization peak temperature (T_p) is given in Table 2.

4.3. Crystal phase development by X-ray diffraction

The results of crystal phase development in BCAS glass after heat treatments at various temperatures between 700 and 1000 °C for different times are summarized in Table 3. $BaSiO_3$ is the first phase to crystallize out in this glass. This is followed by the formation of hexacelsian $BaAl_2Si_2O_8$. The $BaSiO_3$ and hexacelsian were the primary crystalline phases whereas monoclinic celsian ($BaAl_2Si_2O_8$) and (Ba_xCa_y)SiO_4 were also detected as minor phases. Needle-shaped $BaSiO_3$ crystals are formed first followed by the formation of other phases at longer times of heat treatments. Crystallization occurred most rapidly at 800 °C. After 1000 °C heat treatment, all samples were totally amorphous.

4.4. Microstructure

Fig. 2 shows the SEM micrographs at various magnifications taken from a glass specimen heat treated for 5 h at 800 °C. Backscatter SEM micrographs taken from polished cross-sections of glass specimens heat treated at 800 °C for different times are shown in Fig. 3. Barium silicate is first seen as white long elongated crystals growing in the amorphous material in the sample heated for 1 h. After 5 h, hexacelsian becomes visible as darker needle shaped crystals in the amorphous material. The dark round regions are alumina. Gray smooth areas are the residual amorphous glass phase consisting of barium–calcium aluminosilicate. The chemical compositions of various phases were confirmed using EDS analysis. The micrographs of samples heat treated for 10 and 40 h show the crystals of various phases growing and impinging on each other. SEM micrographs of glass samples heat treated for 100 h at 750, 800 and 850 °C are presented in Figs. 4–6, respectively.

SEM micrograph and X-ray dot maps of various elements from the polished cross-section of BCAS glass heat treated at 800 °C for 1 h are shown in Fig. 7. A number of phases are present. Bright elongated dendrite shaped crystals consist of $BaSiO_3$. The dark region in the middle is identified as Al_2O_3.

Table 3
Crystalline phase development in BCAS glass on heat treatments

Heat treatment		Crystalline phases detected from X-ray diffraction					
Temperature (°C)	Time (h)	Amorphous	$BaSiO_3$	Hexacelsian	Celsian	$(Ba_{1.5}Ca_{0.5})SiO_4$	$(Ba_{1.31}Ca_{0.69})SiO_4$
700	20	X					
	50	X	X				
750	3	X					
	5	X	X				
	10	X	X				
	100	X	X	X	X		
800	1	X	X				
	5	X	X	X			
	18	X	X	X		X	
	50	X	X	X		X	
	100	X	X	X			
850	21	X	X	X			
	100	X	X		X		X
900	10	X	X	X			
	100	X	X	X			
1000	10	X					
	50	X					

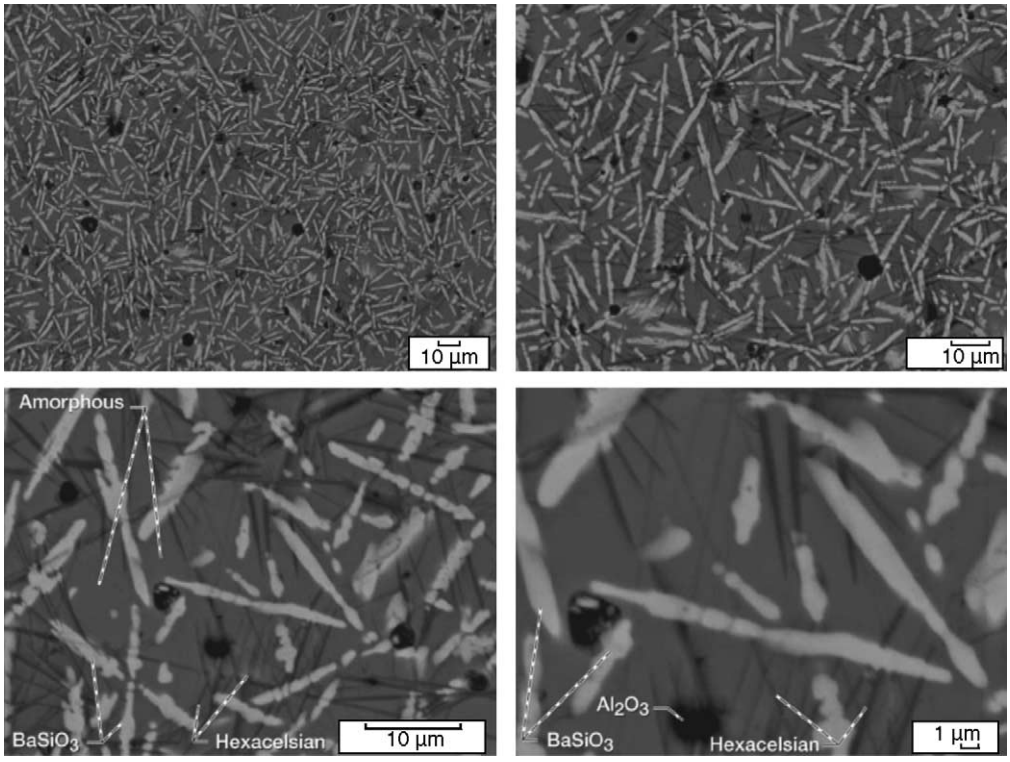

Fig. 2. SEM backscatter micrographs of polished cross-sections of BCAS bulk glass heat treated at 800 °C for 5 h.

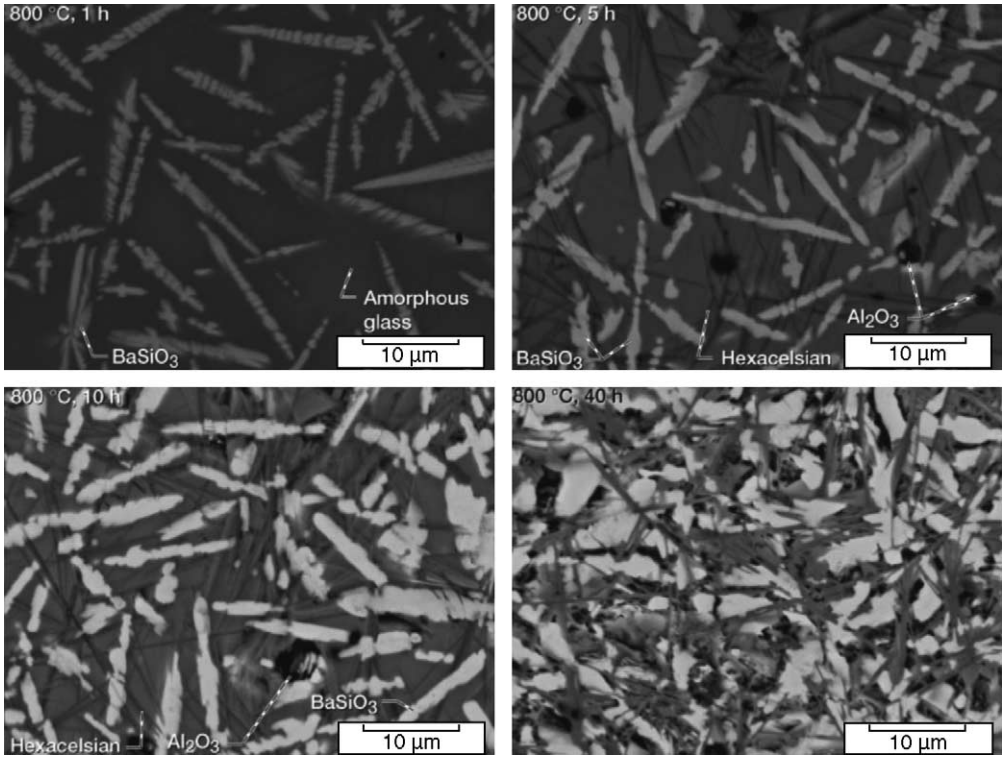

Fig. 3. SEM backscatter micrographs of polished cross-sections of BCAS bulk glass heat treated at 800 °C for various times.

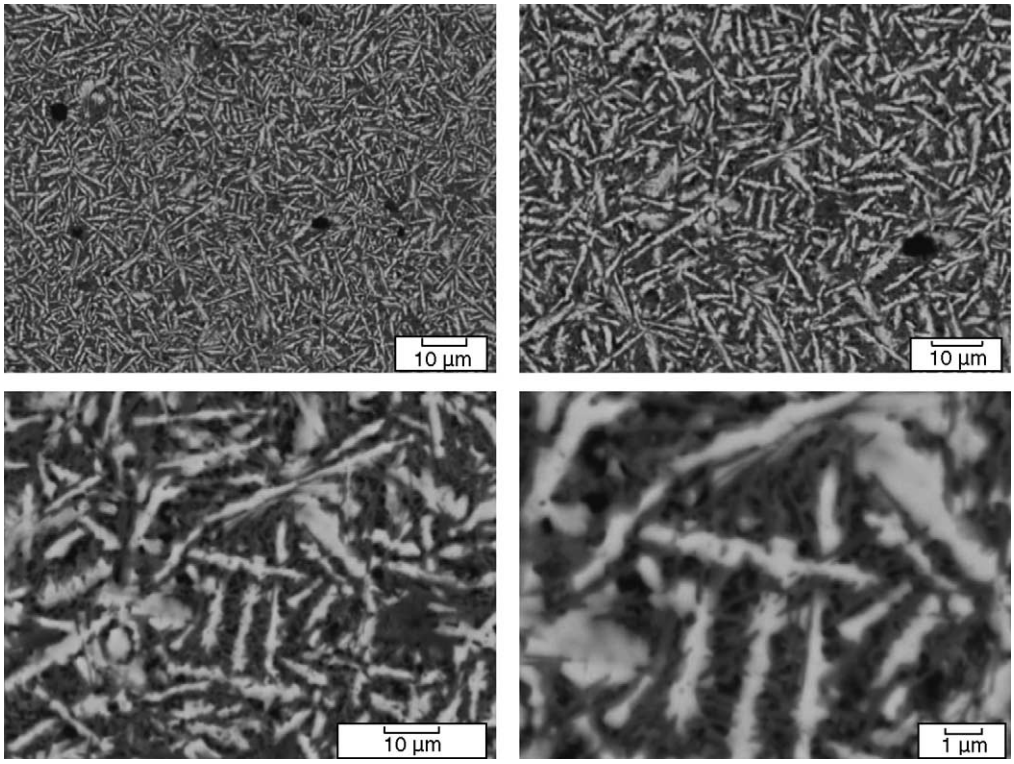

Fig. 4. SEM backscatter micrographs of polished cross-section of BCAS bulk glass heat treated at 750 °C for 100 h.

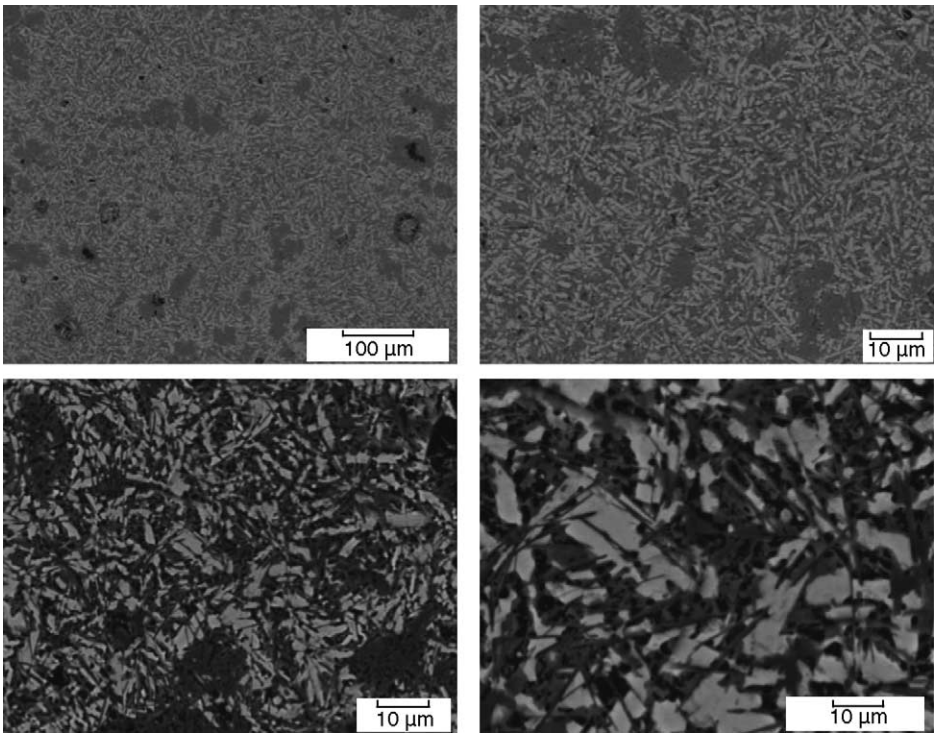

Fig. 5. SEM backscatter micrographs of polished cross-section of BCAS bulk glass heat treated at 800 °C for 100 h.

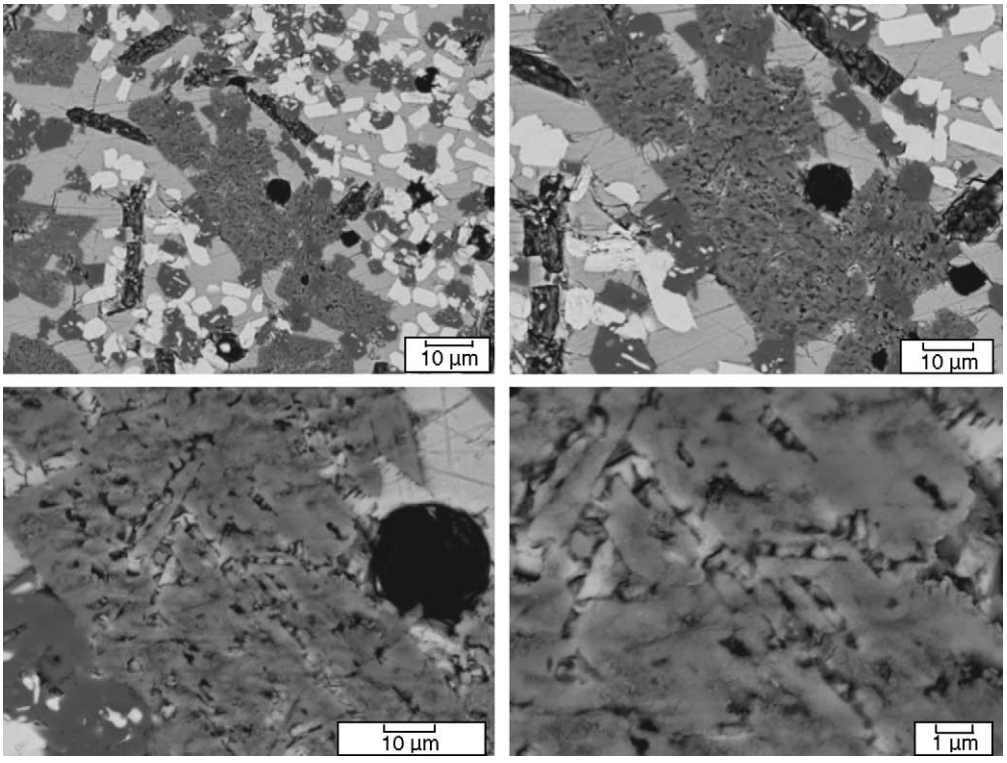

Fig. 6. SEM backscatter micrographs of polished cross-section of BCAS bulk glass heat treated at 850 °C for 100 h.

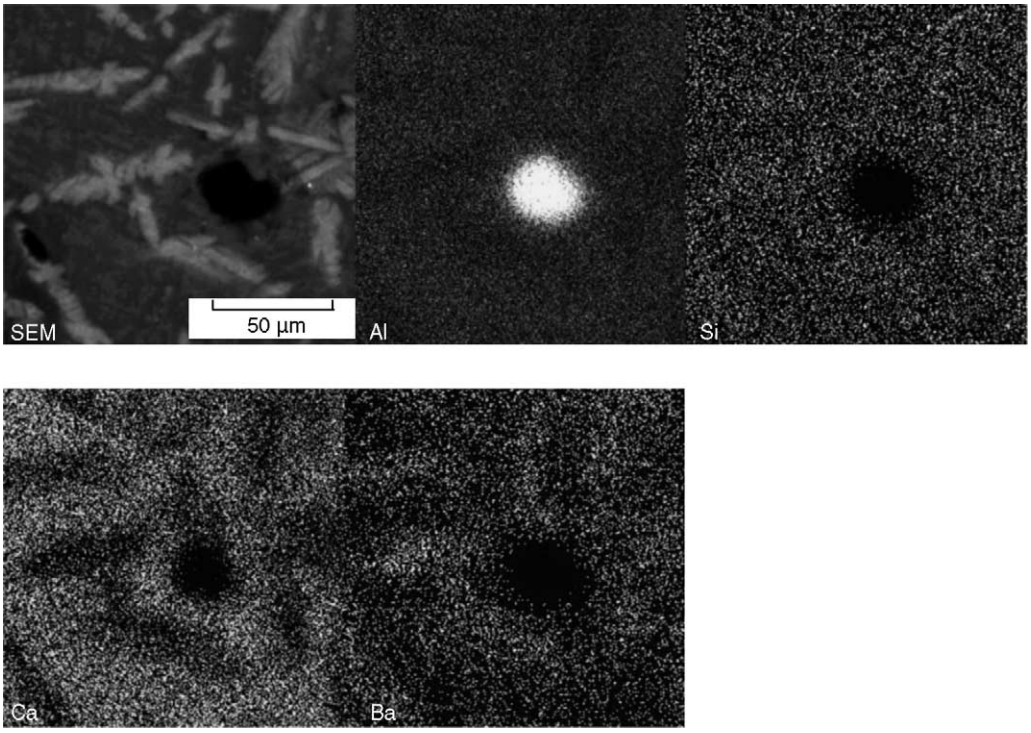

Fig. 7. SEM micrograph and X-ray dot maps of various elements from polished cross-section of BCAS bulk glass heat treated at 800 °C for 1 h.

5. Discussion

The crystallization peak maximum temperature is seen to increase with increase in heating rate (Table 2). The crystallization peak maximum in the DTA or DSC scans corresponds to the temperature at which the rate of transformation of the viscous liquid into crystals becomes maximum. When the crystalline phase has the same composition as the liquid, the transformation rate will depend on the density of crystallization sites. However, when the composition of the crystalline phase is different from that of the liquid, as in the present case, the rate of transformation will be controlled by the rate of diffusion through the viscous liquid and the number of crystallization sites to which diffusion can occur. If the number of nucleation sites is increased, e.g., by using slower heating rates, the peak maximum will occur at a temperature at which the melt viscosity is higher, i.e., at a lower temperature. This explains the increase in T_p with the heating rate (Table 2) observed in the present study.

Plot of $\ln(T_p^2/\theta)$ versus $1/T_p$ for crystallization of the glass is shown in Fig. 8. A linear plot indicates validity of the kinetic model of Bansal et al. [14–16] and validity of the assumptions made in this model. Values of kinetic parameters E and υ obtained from linear least squares fitting of the experimental data are listed in Table 4. The crystallization activation energy of 259 kJ/mol for BCAS glass is much lower than 473–560 kJ/mol, reported earlier for barium aluminosilicate (BAS) and strontium aluminosilicate (SAS) glasses [18,19] as well as 420 kJ/mol for magnesium alumino-borosilicate (MABS) glass [20]. The large difference in activation energy

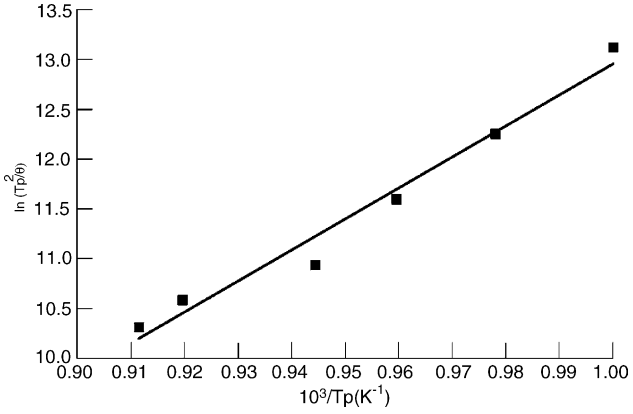

Fig. 8. Plots of $\ln(T_p^2/\theta)$ vs. reciprocal of crystallization peak temperature for BCAS glass powder.

may be due to the different first formed crystalline phases in various glasses. The $BaSiO_3$ crystalline phase is formed first in BCAS glass whereas it was $BaAl_2Si_2O_8$ in BAS, $SrAl_2Si_2O_8$ in SAS and $MgSiO_3$ in MABS glasses. The activation energy of 259 kJ/mol in the present study is probably for the growth of $BaSiO_3$ crystals. The Piloyan plot of $\ln(\Delta y)$

Table 4
Crystallization kinetic parameters for BCAS glass determined by DTA

Parameter	Value
Activation energy, E (kJ/mol)	259
Frequency factor, υ (s^{-1})	2.6×10^{12}
Avrami parameter (n)	2.6

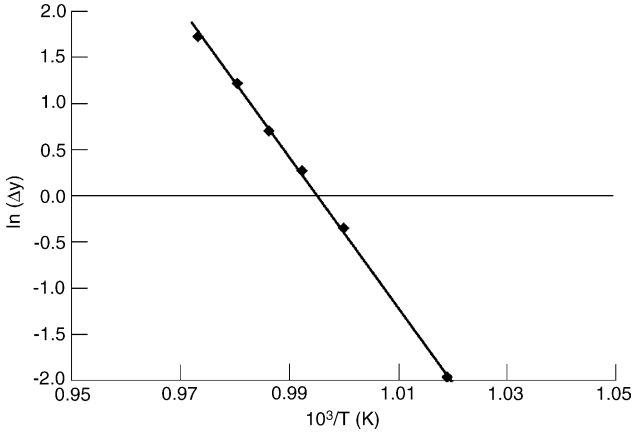

Fig. 9. Piloyan plot for the crystallization of BCAS glass powder for DTA thermogram recorded at a heating rate of 20 K/min.

versus $1/T$ for crystallization of BCAS glass (Fig. 9) is linear. Deviations were observed at higher temperatures, as the Piloyan's equation is valid only in the range $0 < x < 0.2$. The value of n obtained from least squares fitting of linear part of the data to Eq. (6) was 2.6. The value of n depends on the mechanism of the transformation reaction. Possible values of n for various mechanisms based on zero or constant nucleation rate are given in Table 5. If the rate of nucleation is a function of time, so is n; n is higher for a constant nucleation rate than when the nucleation rate increases with time and lies between those for constant and zero nucleation rates when the nucleation rate decreases with time. The n value of 2.6 in the present study probably corresponds to the two-dimensional growth of $BaSiO_3$ as XRD results indicated that this phase is formed first on heat treatment of BCAS glass. This is further supported by the SEM micrographs in Figs. 2–4, which show two-dimensional growth of needle-shaped crystals of $BaSiO_3$ on heat treatment of the glass.

The $BaSiO_3$ phase crystallizes most readily in BCAS glass. On further heat treatment, hexagonal and monoclinic $BaAl_2Si_2O_8$ and various barium–calcium silicates ($(Ba_xCa_y)SiO_4$) phases are also formed. Rate of crystallization depends on the heat treatment temperature. CTE of the devitrified glass after long-term treatments at the operating temperature of SOFC, not just that of the original glass, should match the CTE of other SOFC components (electrolyte, cathode, anode and interconnect) to minimize thermal stresses.

Table 5
Possible values of n for various mechanisms [16,17]

Constant nucleation rate		Growth of constant number of nuclei (zero nucleation rate)	
Reaction mechanism	n	Reaction mechanism	n
One-dimensional growth	2	One-dimensional growth	1
Two-dimensional growth	3	Two-dimensional growth	2
Three-dimensional growth	4	Three-dimensional growth	3

6. Summary

Crystallization kinetics of BCAS glass have been studied by DTA. Crystallization activation energy was determined to be 259 kJ/mol. Development of crystalline phases in the glass, after isothermal heat treatments at various temperatures for different times, has been investigated by X-ray diffraction and microstructural characterization. On heat treatment at 700 °C, $BaSiO_3$ crystallizes first from the glass. This is followed by the formation of hexagonal and monoclinic $BaAl_2Si_2O_8$ and barium–calcium silicate ($(Ba_xCa_y)SiO_4$) phases when treated at higher temperatures and/or longer times. After 1000 °C heat treatment, the samples were totally amorphous.

7. Conclusions

Properties of the barium–calcium aluminosilicate glass of this study are compatible with those of the solid oxide fuel cell components. This glass does not fully crystallize even after long-term heat treatments at 750–900 °C, the operating temperature for SOFC. Devitrification of the glass seal over a long period of time during operation of the SOFC would generate thermal stresses in the seal and may have adverse effects on its mechanical performance. This may lead to cracking of the seal, resulting in mixing of the fuel and the oxidant gases. CTE of the devitrified glass after long-term treatments at the operating temperature of SOFC, not just that of the original glass, should match the CTE of other SOFC components (electrolyte, cathode, anode and interconnect) to minimize thermal stresses.

Acknowledgments

Thanks are due to John Setlock for technical assistance during this work, Anna Palczer for DTA analysis and Ralph Garlick for X-ray diffraction measurements. Eleanor Gamble was a student intern from Purdue University at NASA Glenn during the summer of 2003.

References

[1] N.Q. Minh, J. Am. Ceram. Soc. 76 (1993) 563.
[2] K. D. Meinhardt, J. D. Vienna, T. R. Armstrong, L. R. Pederson, Glass-Ceramic Joint and Method of Joining, U.S. Patent 6,532,769 March 18, 2003.
[3] K.L. Ley, M. Krumpelt, R. Kumar, J.H. Meiser, I. Bloom, J. Mater. Res. 11 (1996) 1489.

[4] S.-B. Sohn, S.-Y. Choi, G.-H. Kim, H.-S. Song, G.-D. Kim, J. Am. Ceram. Soc. 87 (2004) 254.
[5] R.E. Loehman, H.P. Dumm, H. Hofer, Ceram. Eng. Sci. Proc. 23 (2002) 699.
[6] K. Eichler, G. Solow, P. Otschik, W. Schaffrath, J. Eur. Ceram. Soc. 19 (1999) 1101.
[7] P. Geasee, R. Conradt, T. Schwickert, A. Janke, J. Remmel, F. Tietz, Proc. Int. Congr. Glass 2 (2001) 47 (extended abstracts).
[8] R. Zheng, S.R. Wang, H.W. Nie, T.-L. Wen, J. Power Sources 128 (2004) 165.
[9] Z. Yang, K.D. Meinhardt, J.W. Stevenson, J. Electrochem. Soc. 150 (2003) A1095.
[10] Z. Yang, J.W. Stevenson, K.D. Meinhardt, Solid State Ionics 160 (2003) 213.
[11] W.A. Johnson, R.F. Mehl, Trans. Am. Inst. Min. Met. Eng. 135 (1939) 416.
[12] M. Avrami, J. Chem. Phys. 7 (1939) 1103;
M. Avrami, J. Chem. Phys. 8 (1940) 212;
M. Avrami, J. Chem. Phys. 9 (1941) 177.
[13] H.J. Borchard, J. Inorg. Nucl. Chem. 12 (1960) 252.
[14] N.P. Bansal, R.H. Doremus, J. Thermal Anal. 29 (1984) 115.
[15] N.P. Bansal, R.H. Doremus, A.J. Bruce, C.T. Moynihan, J. Am. Ceram. Soc. 66 (1983) 233.
[16] N.P. Bansal, A.J. Bruce, R.H. Doremus, C.T. Moynihan, J. Non-Cryst. Solids 70 (1985) 379.
[17] G.O. Piloyan, I.D. Rybachikov, O.S. Novikova, Nature 212 (1966) 1229.
[18] N.P. Bansal, M.J. Hyatt, J. Mater. Res. 4 (1989) 1257.
[19] M.J. Hyatt, N.P. Bansal, J. Mater. Sci. 31 (1996) 172.
[20] D. Bahadur, N. Lahl, K. Singh, L. Singheiser, K. Hilpert, J. Electrochem. Soc. 151 (2004) A558.